

**Investigation of Nano-Scale Oxide Inclusions in 316L Stainless Steel Processed by
Powder Bed Additive Manufacturing**

Fuyao Yan^{1,*}, Wei Xiong^{2,*}, Eric Faierson³, Gregory B. Olson^{1,*}

1. Department of Materials Science and Engineering, Northwestern University, Evanston,
Illinois 60201, USA

2. Department of Mechanical Engineering and Materials Science, University of
Pittsburgh, Pittsburgh, PA 15261, USA

3. Quad City Manufacturing Laboratory, Rock Island, IL 61299, USA

* Corresponding authors:

Email: fuyaoyan2018@u.northwestern.edu (F.Yan), weixiong@pitt.edu (W. Xiong), g-olson@northwestern.edu (G.B. Olson)

Address: 2220 Campus Drive, Cook Hall 2036, Evanston, IL 60208, USA

Tel: +1 847 491 5222

Fax: +1 847 491 7820

Abstract

Nano-scale MnO-SiO₂ rhodonite particles were observed in 316L stainless steel processed by selective laser melting. The *in-situ* formed rhodonite particles in the as-built alloys were found to act as Zener-pinning particles providing dragging force to retard grain growth, and thus further enhance strength, via the comparisons of Hall-Petch effects between SLM 316L and commercial wrought 316L under the 1200 °C isothermal heat treatment. MnO-SiO₂ rhodonite particles were observed to transform to the stable MnO-Cr₂O₃ spinel particles at 1200 °C, which can be explained by employing thermodynamic calculations. The present work demonstrates a possible solution to turn the detrimental oxide particles as inclusions into grain refine particles phase by post-process optimization.

Keywords: selective laser melting; 316L austenitic stainless steel; oxide inclusion; strengthening; Zener pinning

Additive manufacturing (AM) has received a great attention in the past few years for the potential of building complex parts layer-by-layer without design constraints as in conventional manufacturing [1]. Selective laser melting (SLM) is a powder-bed AM technique, which utilizes a high power laser to selectively melt and fuse the pre-laid powders in a layer-by-layer manner. The whole process is conducted in a closed chamber which is often filled with argon gas or nitrogen gas to provide an inert atmosphere to prevent oxidation of metal pieces at elevated temperatures [2]. Unfortunately, oxidation is inevitable, since there are always oxide impurities in the powders and an oxygen partial pressure in the building chamber [3]. The detrimental effects of oxide inclusions on weld-metal properties have long been recognized in the welding community. Deoxidation reactions and mechanisms for the formation of non-metallic inclusions in steel during solidification in the casting and welding process have also been studied extensively [4–6]. However, there are few publications that cover the study of oxide inclusions in AM metal builds. Thijs *et al.* [7] found large Ti and Al oxides (10~100 μm) in maraging steel 18Ni(300) SLM parts. Meanwhile, nano-scale Si-rich oxide particles were discovered in laser-melted 316L stainless steel, along with excellent tensile properties in the as-built condition. Therefore, the idea of in-situ formation of oxide dispersion strengthening (ODS) steel by AM was proposed [8,9]. However, more data is needed to clarify the strengthening effects of oxide nano-inclusions. Additionally, as post heat treatment (e.g.

hot isostatic pressing) is commonly performed after AM processes, it is essential to investigate the evolution of oxide inclusions during subsequent heat treatment.

316L stainless steel is a single phase (austenite) alloy, it is rather straightforward to study the effects of oxide inclusions. In this study, 316L stainless steel was built by SLM and was then isothermally heat-treated at 1200 °C. The stability and the kinetics of oxide particles, along with their impacts on grain structure and mechanical properties were studied.

316L powders (16 - 44 μm) were produced by Carpenter Powder Products Inc. with the composition listed in [Table 1](#). A 10 mm x 20 mm x 10 mm cube was fabricated by the EOS M270 powder bed fusion system, with 180 W laser power, 1000 mm/s scan speed, 180 μm beam diameter, 0.02 mm layer thickness and 0.09 mm hatch spacing. Oxygen content was measured by the inert gas fusion method for the as-built alloy, which was cut into 3 mm x 10 mm x 3 mm samples for further heat treatment. Commercial 316L alloy in the form of cold-rolled square bar (10 mm x 10 mm x 300 mm) was purchased from TA Chen Stainless Pipe Co., LTD. The as-received material ([composition is given in Table 1](#)) was in the rolled and annealed state according to the ASTM A484-13a standard. Pieces of both SLM and commercial specimens were encapsulated in quartz tubes under vacuum, and then argon is back-filled into the tube until a pressure of 10^{-4} to 10^{-2} torr is

reached. Samples were heat treated at 1200 °C for 0.5 hour, 1 hour and 2 hours, followed by water quenching. One piece of commercial 316L specimen was heat treated at 1200 °C for 12 hours in order to establish a larger grain size. An array of 36 Vickers hardness indentations was performed on all as-polished surfaces by a Clemex MMT microhardness tester, with a load of 100g and dwell time of 10 seconds. Revealing grain boundaries was aided by a thin oxide layer, obtained by a high-temperature exposure to air for a couple of seconds. Optical metallography was applied for grain structures analysis before electron microscopy. Grain size was determined by the intercept method based on the ASTM E112-12 standard. SLM 316L samples were further vibratory polished with 0.06 µm colloidal silica for 2 hours before the EBSD examination, which was performed in an FEI Quanta ESEM. A thin layer perpendicular to the build direction was taken from the bottom part of the SLM 316L samples in the as-built state and heat-treated state. JOEL JEM-2100 FasTEM and Hitachi HD-2300 Dual EDS Cryo STEM equipped with dual energy-dispersive x-ray spectroscopy (EDX) and electron energy loss spectroscopy (EELS) were used for microstructural analysis on thin foil samples prepared by electropolishing.

Evolution of SLM 316L grain structures during isothermal heat treatment under 1200 °C is illustrated by inverse pole figure color map using electron back scattering diffraction (EBSD) techniques, shown in [Figure 1](#). As implied by [Figure 1\(a\)](#), grains in the as-built

condition are mostly columnar along the build direction and are highly textured along $\langle 110 \rangle$ directions. The bi-modal distribution of grains and less-textured smaller equiaxed grains shown in [Figure 1\(b\)](#) indicate the release of residual stress in the form of recrystallization after 30 min heat treatment at 1200 °C. As time increases, the smaller equiaxed grains keep growing, consuming textured grains (green area in [Figure 1\(b\)-\(d\)](#)), and the number of twins in the FCC structure increases with annealing time. The $\{110\}$ pole figures for the austenite phase imply that the texture structure gradually disappeared after 30-minute annealing.

Thin foils from the bottom layer (x-y plane) of SLM 316L in the as-built condition were observed by (S)TEM in both bright field and Z-contrast mode. As shown in [Figure 2\(a\)](#), arrays of cellular structures were clearly evident in the bright field mode, with high density of dislocations at the cell boundaries. In the Z-contrast mode, highly dispersed nano-particles were observed mostly on cell boundaries, as shown in [Figure 2\(b\)](#). Since these particles were found to be less than 100 nm in the as-built state, they can be expected to act as effective Zener-pinning particles for grain refinement during heat treatment. Nano-diffraction was able to shed electron beam on a specific particle for crystal structure analysis. The diffraction pattern as in [Figure 2\(b\)](#) includes a FCC structured-pattern for austenite matrix and a set of extremely complex diffraction spots, indicating the particles possessing a low-symmetry crystal structure. Line scans across

the spherical particles were performed by EDX to determine oxide composition variations. It was found that such particles were rich in Mn and Si, as shown in [Figure 2\(c\)](#). Since EDX has limitations in detecting light-weight elements, EELS was then used revealing a significant difference in the peaks of Si, O and Mn between the matrix and the particle, as shown in [Figure 2\(d\)](#). The Si peak is not shown in the particle EELS spectrum, since its energy loss is not on the same order of magnitude of that of O and Mn. Since common oxides that are rich in Mn and Si in Mn/Si deoxidized steels are usually rhodonite (MnSiO_3) [5,6], a type of mixed oxides (MnO-SiO_2) with a triclinic crystal structure, the particles in the as-built SLM 316L alloy should be interpreted as rhodonite. The morphologies and compositions of oxide particles were then observed after each annealing step. After annealing for 1 hour, the fraction of spherical particles decreased significantly, with the emergence of a considerable number of prismatic particles, as shown in [Figure 2\(e\)](#). All particles were found to be prismatic and rich in Mn and Cr (see [Figure 2\(f\)](#)). The diffraction pattern of the particles identified the particles to be MnCr_2O_4 ($\text{MnO-Cr}_2\text{O}_3$) spinel consistent with JCPDS card No. 75-1614.

As indicated in [Figure 3](#), SLM 316L in the as-built condition exhibits the highest hardness, and the hardness drops as it is heat-treated. By constructing a Hall-Petch relationship among the heat-treated SLM 316L specimens, the extrapolation still falls short of the hardness in the as-built state. Since grain boundary strengthening is

represented by the Hall-Petch relationship, the difference in hardness is primarily attributed to the strengthening effect by high-density dislocations in the form of cell boundaries, as shown in [Figure 2\(a\)](#). As the as-built material is heat-treated, dislocations gradually recover and annihilate, resulting in a significant drop in hardness. This is in accordance with the tensile property comparisons between the as-built and heat-treated AM 316L in previous research [8,9]. Another Hall-Petch relationship was constructed for the heat-treated commercial rolled and annealed 316L, with a smaller slope compared with that for the heat-treated SLM 316L. By accounting for the effect of grain size, the higher hardness in the heat-treated SLM 316L is mainly attributed to the strengthening of finely dispersed oxide particles. The intercept of the two lines indicates where the strengthening effect of oxide particles become negligible as particles coarsen with long-time heat treatment.

In order to understand the phase transition of oxide particles observed in isothermal heat treatment at 1200 °C, phase relations were studied based on thermodynamic calculations using the Thermo-Calc software. With the composition of 316L SS, an equilibrium step diagram was constructed using the TCFE9 thermodynamic database, represented in [Figure 4\(a\)](#). It predicts that, at 1200 °C, the equilibrium phases are FCC (austenite), spinel and MnS. Since MnS is of low phase fraction, the MnS was not seen experimentally. Instead, Mn was mostly partitioned into oxide particles. The intriguing phase transition

from rhodonite to spinel can be explained by calculating a metastable phase diagram as given in [Figure \(b\)](#), where the equilibrium spinel phase are dormant, and the oxygen-rich rhodonite phase is predicted with a comparable phase fraction as stable spinel. Since rapid solidification accompanies the AM process, the metastable rhodonite phase with a lower interfacial energy [10] has a higher rate of nucleation during solidification compared to the stable spinel phase. During isothermal heat treatment at 1200 °C, Cr gradually diffuses to the oxide particles, and rhodonite gradually transforms to spinel, with morphology changing from spherical to prismatic [11,12].

Compared with materials designs for conventional manufacturing process which deliberately introduces Zener-pinning grain particles, such as MC (M = Ti, V, Nb) carbides in steels [13] and silicides in titanium alloys [14], AM processes can take advantage of the residual oxygen in the chamber to form nano-scale oxide dispersions due to rapid solidification [15]. In this case, there is no need for an extra heat treatment step for the formation of Zener-pinning particles as in the conventional processes. Further studies will apply kinetic simulations of oxide evolution during AM and post heat treatment. With quantified distributions of oxide particles, it should be possible to predict strengthening contributions by Orowan strengthening and grain boundary strengthening through the Zener-Gladman pinning model [16].

This work was supported by National Institute of Standards and Technology (NIST) through award number 70NANB13H194. Quad City Manufacturing Lab fabricated the materials. The work made use of the MatCI facility and EPIC facility which receive support from the MRSEC Program (NSF DMR-1121262) of the Materials Research Center at Northwestern University. Microhardness testing was performed in QuesTek Innovations, LLC.

References

- [1] D. Herzog, V. Seyda, E. Wycisk, C. Emmelmann, *Acta Mater.* 117 (2016) 371–392.
- [2] B. Song, S. Dong, S. Deng, H. Liao, C. Coddet, *Opt. Laser Technol.* 56 (2014) 451–460.
- [3] K. Saeidi, L. Kvetková, F. Lofaj, Z. Shen, T. Kaito, T. Narita, S. Jiguang, T. Nishida, M. Fujiwara, *RSC Adv.* 5 (2015) 20747–20750.
- [4] C.S. Chai, T.W. Eagar, *Metall. Trans. B* 12 (1981) 539–547.
- [5] A.O. Kluken, Ø. Grong, *Metall. Trans. A* 20 (1989) 1335–1349.
- [6] S.S. Babu, S.A. David, J.M. Vitek, K. Mundra, T. DebRoy, *Mater. Sci. Technol.* 11 (1995) 186–199.

- [7] L. Thijs, J. Van Humbeeck, K. Kempen, E. Yasa, J. Kruth, M. Rombouts, in:, *Innov. Dev. Virtual Phys. Prototyp.*, CRC Press, 2011, pp. 297–304.
- [8] Y. Zhong, L. Liu, S. Wikman, D. Cui, Z. Shen, *J. Nucl. Mater.* 470 (2016) 170–178.
- [9] M. Montero Sistiaga, S. Nardone, C. Hautfenne, J. Van Humbeeck, in:, *Proc. 27th Annu. Int. Solid Free. Fabr. Symp. 2016 - an Addit. Manuf. Conf.*, Austin, TX, United states, 2016, pp. 558–565.
- [10] Ø. Grong, *Metallurgical Modelling of Welding*, 2nd ed., Institute of Materials, London, United Kingdom, 1997.
- [11] H. Shibata, T. Tanaka, K. Kimura, S.-Y. Kitamura, *Ironmak. Steelmak.* 37 (2010) 522–528.
- [12] H. Shibata, K. Kimura, T. Tanaka, S. Kitamura, *ISIJ Int.* 51 (2011) 1944–1950.
- [13] G.B. Olson, in:, G.B. Olson, M. Azrin, E.S. Wright (Eds.), *Innov. Ultrahigh-Strength Steel Technol.*, U.S. Army Laboratory Command, Materials Technology Laboratory, Watertown, Massachusetts, 1987, pp. 3–66.
- [14] D. Weinem, J. Kumpfert, M. Peters, W.A. Kaysser, *Mater. Sci. Eng. A* 206 (1996) 55–62.
- [15] G.B. Olson, R.G. Bourdeau, in:, S.K. Das, B.H. Kear, C.M. Adam (Eds.), *Rapidly Solidified Alloy.*, TMS-AIME, Warrendale, Pennsylvania, USA, 1985, pp. 185–201.

- [16] T. Gladman, Proc. R. Soc. London A Math. Phys. Eng. Sci. 294 (1966).

Figures and Captions

Figure 1. Inversed pole figure color maps and (110) build direction pole figures for the austenite phase in SLM 316L during isothermal heat treatment at 1200 °C. (a) As-built condition; (b) Heat-treated for 30 minutes; (c) Heat-treated for 1 hour; (d) Heat-treated for 2 hours.

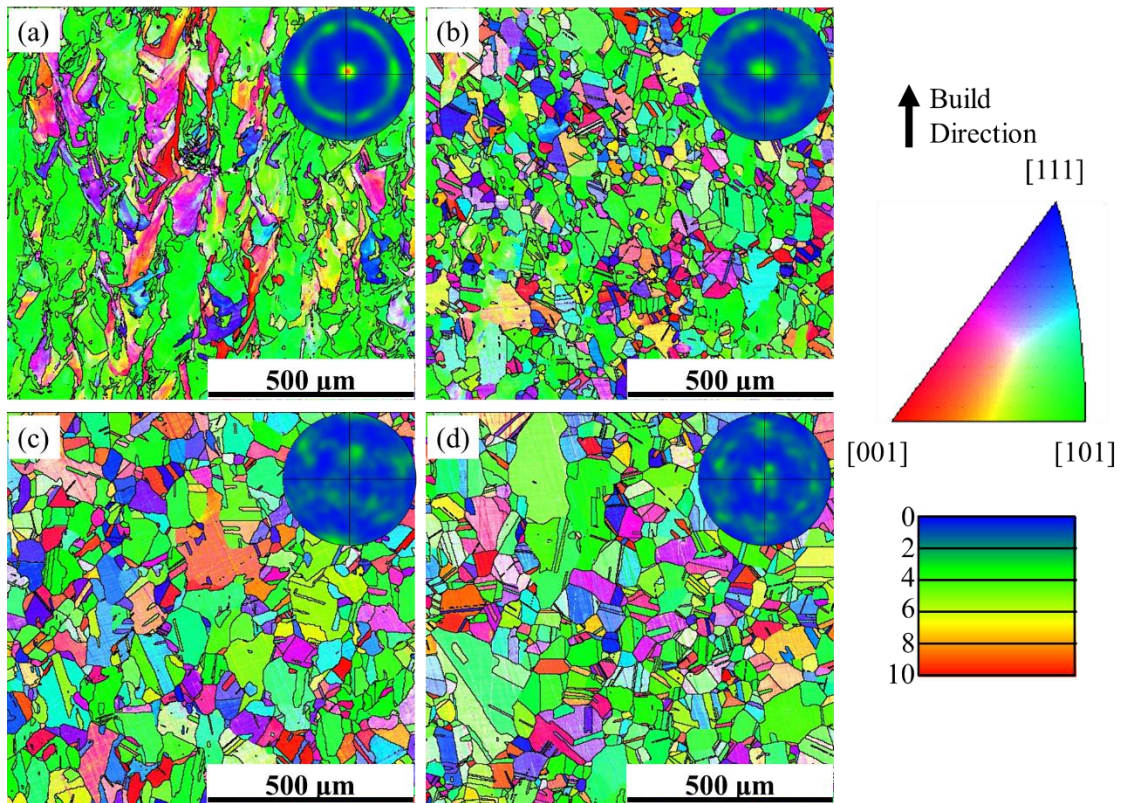


Figure 2. Morphology, composition and crystal structure of oxide particles in the as-built and heat-treated SLM 316L. (a) Cellular structure in the as-built condition (bright field); (b) Spherical particles along cell boundaries in the as-built condition (Z-contrast), with the nano-diffraction pattern for the spherical particles; (c) EDX linear scan over a spherical particle in the as-built condition showing the particles rich in Si and Mn; (d) EELS spectrum for particle and matrix in the as-built condition; (e) Prismatic particles distributed in the SLM 316L heat-treated at 1200 °C for 1 hour, with the nano-diffraction pattern for the prismatic particles; (f) EDX linear scan over a prismatic particle showing the particles rich in Cr and Mn.

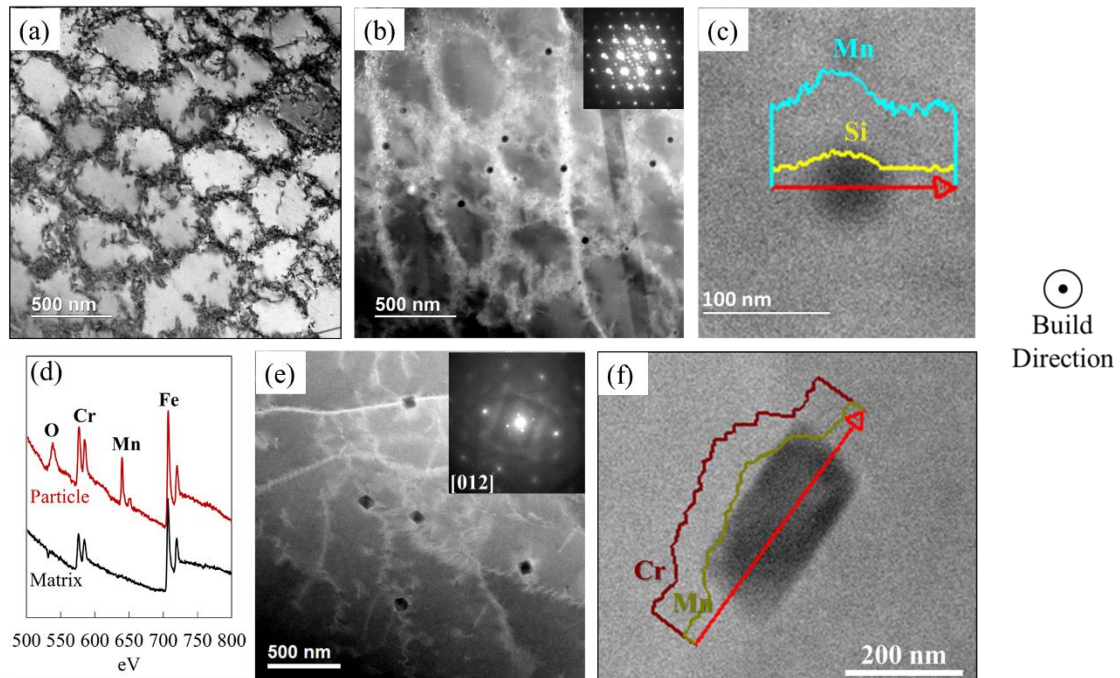


Figure 3. Relationship of hardness and grain size for SLM 316L in the as-built state (black), SLM 316L in the heat-treated state (blue) and commercial 316L in the heat-treated state (red).

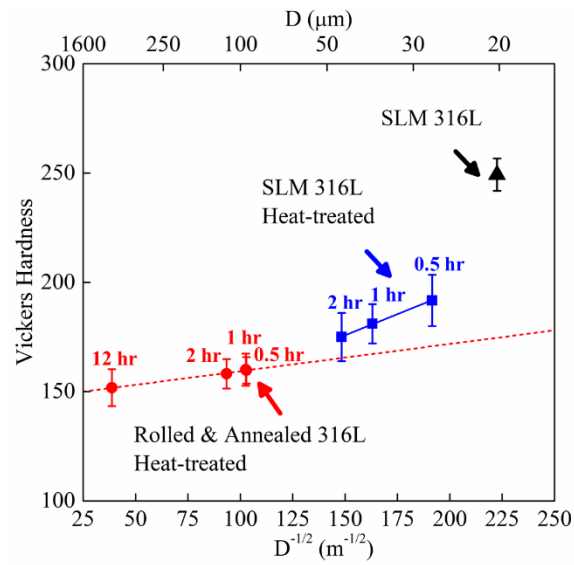
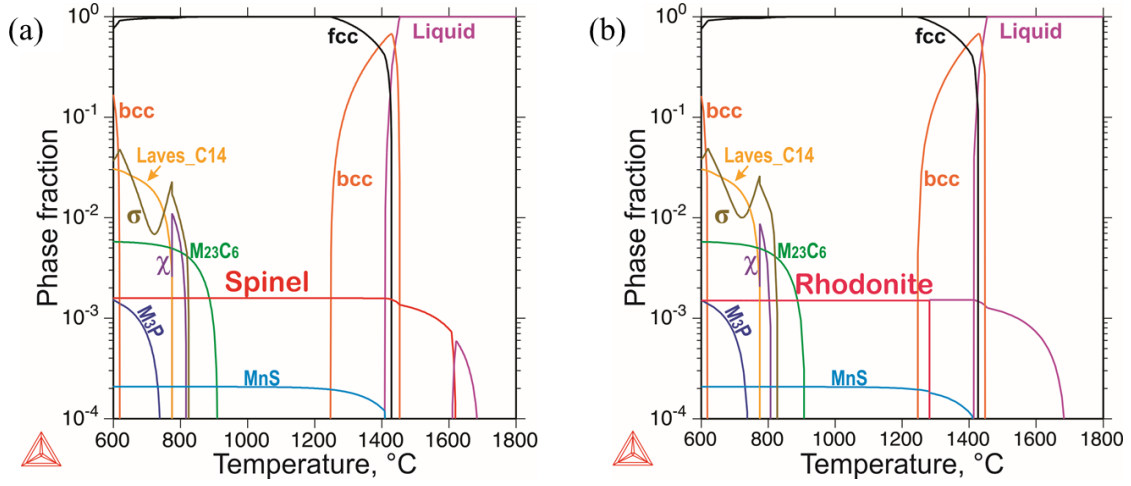


Figure 4. Step diagrams for 316L with the composition Fe-16.3Cr-10.3Ni-2.09Mo-1.31Mn-0.49Si-0.026C-0.006S-0.026P-0.026O in wt.%. (a) Equilibrium step diagram; (b) metastable step diagram with spinel phase dormant.



Table

Table 1 Composition of 316L powders and 316L commercial alloy (in wt.%)

	Fe	Cr	Ni	Mo	Mn	Si	Cu	C	S	P	O
Powder	Bal	16.3	10.3	2.09	1.31	0.49	--	0.026	0.006	0.026	0.026
Commercial alloy	Bal	16.69	10.09	2.01	1.75	0.41	0.52	0.019	0.0256	0.026	--